Eur. Phys. J. C (2021) 81:261
https://doi.org/10.1140/epjc/s10052-021-08994-0

THE EUROPEAN PHYSICAL JOURNAL C

Regular Article - Experimental Physics

Search for long-lived particles decaying to $e^{\pm}\mu^{\mp}\nu$

LHCb Collaboration[⋆]

CERN, 1211 Geneva 23, Switzerland

Received: 7 December 2020 / Accepted: 22 February 2021 / Published online: 26 March 2021

Abstract Long-lived particles decaying to $e^{\pm}\mu^{\mp}\nu$, with masses between 7 and 50 GeV/c^2 and lifetimes between 2 and 50 ps, are searched for by looking at displaced vertices containing electrons and muons of opposite charges. The search is performed using 5.4 fb^{-1} of pp collisions collected with the LHCb detector at a centre-of-mass energy of $\sqrt{s} = 13$ TeV. Three mechanisms of production of long-lived particles are considered: the direct pair production from quark interactions, the pair production from the decay of a Standard-Model-like Higgs boson with a mass of 125 GeV/c^2, and the charged current production from an on-shell W boson with an additional lepton. No evidence of these long-lived states is obtained and upper limits on the production cross-section times branching fraction are set on the different production modes.

1 Introduction

A variety of models beyond the Standard Model (SM) feature the existence of new massive particles with lifetimes that can be long, compared to the SM particles at the weak scale. These so-called long-lived particles (LLP) appear, for example, in Supersymmetry or extensions to the SM that predict right-handed neutrinos [1]. The study presented in this paper focuses on the search for decays of neutral LLPs using three production mechanisms: direct pair production (DPP), pair production from the decay of a SM-like Higgs boson with a mass of 125 GeV/c^2 (HIG), and from charged current (CC) processes. Diagrams for each production mode are shown in Fig. 1. The production of LLPs from the decay of a SM-like Higgs boson has been studied in several searches conducted by the CMS, ATLAS and LHCb experiments, using LLP decays to light-flavour jets [2–6], b-quark jets [7] and light leptons [8,9]. In this study the LLP can be a neutralino $\tilde{\chi}_0^1$, in R-parity-violating supersymmetric models [10], or a right-handed neutrino N decaying to two charged leptons and a neutrino [11–13]. Searches for LLP$\to e^{\pm}\mu^{\mp}\nu$ decays have been performed by the ATLAS experiment in the context of Supersymmetry [14], and also with right-handed neutrinos [15].

The first direct LLP$\to e^{\pm}\mu^{\mp}\nu$ search at the LHCb experiment is presented in this paper. The LHCb detector probes the forward rapidity region that is only partially covered by the other LHC experiments, and triggers on particles with low transverse momenta, which allows the experiment to explore relatively small LLP masses. In the present study, displaced vertices consisting of an electron and a muon of opposite charges are searched for in pp collisions at a centre-of-mass energy of $\sqrt{s} = 13$ TeV, using a data sample corresponding to an integrated luminosity of 5.38 ± 0.11 fb^{-1} collected with the LHCb detector in 2016–2018. The momentum of the neutrino in the final state can be partly reconstructed from the misalignment between the LLP flight direction and the momentum of the electron and muon system. The explored masses of the LLP ($m_{\rm LLP}$) range from 7 to 50 GeV/c^2 and lifetimes ($\tau_{\rm LLP}$) range from 2 to 50 ps. This search enlarges the domain of searches for heavy LLPs at LHCb, which previously probed for displaced jets [4–6] or displaced dimuons [16–18].

2 Detector description

The LHCb detector [19,20] is a single-arm forward spectrometer covering the pseudorapidity range $2 < \eta < 5$, designed for the study of particles containing b or c quarks. The detector includes a high-precision tracking system consisting of a silicon-strip vertex detector surrounding the pp interaction region (VELO), a large-area silicon-strip detector located upstream of a dipole magnet with a bending power of about 4 Tm, and three stations of silicon-strip detectors and straw drift tubes, placed downstream of the magnet. The tracking system provides a measurement of momentum, p, of charged particles with a relative uncertainty that varies from 0.5% at low momentum to 1.0% at 200 GeV/c. The minimum distance of a track to a primary pp collision vertex

⋆ e-mail: matthieu.marinangeli@gmail.com

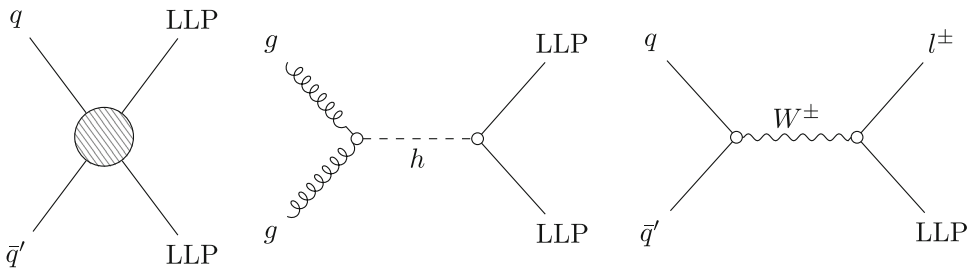

Fig. 1 Production modes of the LLP considered in this search. From left to right: direct pair production (DPP), decay of a SM-like Higgs with a mass of 125 GeV/c^2 produced by gluon-gluon fusion (HIG) and production by charged current (CC)

(PV), the impact parameter (IP), is measured with a resolution of $(15 + 29/p_{\mathrm{T}})$ μm, where p_{T} is the component of the momentum transverse to the beam axis, in GeV/c. Different types of charged hadrons are distinguished using information from two ring-imaging Cherenkov detectors. Photons, electrons and hadrons are identified by a calorimeter system consisting of scintillating-pad and preshower detectors, an electromagnetic calorimeter (ECAL) and a hadronic calorimeter (HCAL). Muons are identified by a system composed of alternating layers of iron and multiwire proportional chambers.

The online event selection is performed by a trigger, which consists of a hardware stage based on information from the calorimeter and muon systems, followed by a software stage that carries out a full event reconstruction. During data taking an alignment and calibration of the detector is performed in near real-time and used in the software trigger [21]. Events from pp collisions fulfilling the muon or electron trigger are studied. At the hardware level the muon trigger requires a muon track identified by matching hits in the muon stations, for the electron trigger a cluster in the ECAL with large transverse energy deposit is required. At the software level the muon trigger selects muons with a minimum p_{T} of 10 GeV/c, the electron trigger selects electrons with a minimum p_{T} of 15 GeV/c.

3 Simulation

Simulated samples of LLP $\to e^{\pm}\mu^{\mp}\nu$ events are used to design and optimise the signal selection and to estimate the detection efficiency, but also for the construction of the signal model. Parton-level events with LLPs are generated at leading order with MadGraph [22] using Universal FeynRules Outputs (UFO) [23] for long-lived particle searches following Ref. [1]. For the DPP and HIG mechanisms, the UFO for the minimal supersymmetric standard model with R-parity violation [10] is chosen, and in this framework the signal is represented by the lightest neutralino $\tilde{\chi}_0^1$. For the CC production the UFO of the Left-Right Symmetric model [24–26] is used, and here the LLP is represented by a heavy neutrino produced from an on-shell W boson. For all three modes, the LLP is allowed to decay into an electron and a muon with opposite charges, and a neutrino. The decay of the LLP is performed through the MadSpin package [27]. The parton shower of the events is simulated with Pythia8 [28,29] using a specific LHCb configuration [30] and using the CTEQ6 leading-order set of parton density functions [31]. The interaction of the particles with the detector and its response are implemented using the Geant4 toolkit [32,33] as described in Ref. [34]. Signal events with $m_{\mathrm{LLP}} = 7$, 10, 15, 20, 30, 38 and 50 GeV/c^2 and $\tau_{\mathrm{LLP}} = 2$, 5, 10, 25 and 50 ps are generated.

Samples are also generated for background studies and cross checks, although the background estimate in this study is based on data. The most relevant background in this analysis is from $b\bar{b}$ events. Two distinct topologies are observed with the two leptons from the same jet or from two different jets, as discussed in Sect. 5. Events generated from $gg/q\bar{q} \to b\bar{b}$ processes with Pythia8, with at least one muon with $p_{\mathrm{T}} > 10$ GeV/c in the LHCb acceptance are simulated and required to satisfy the muon trigger criteria.

4 Signal selection

The LLP $\to e^{\pm}\mu^{\mp}\nu$ candidates are reconstructed from the combination of a muon and an electron candidate of opposite charges forming a good-quality vertex within the VELO detector. The following selection of the candidates is developed and optimised using the DPP samples for each pair of m_{LLP} and τ_{LLP} values. This selection is also adopted for the study of the HIG and CC processes.

The muon and electron candidates are required to have $p_{\mathrm{T}} > 1.6$ GeV/c and $p > 10$ GeV/c. The measured momentum of the electron candidates is corrected for the loss of energy due to bremsstrahlung [35]. The muon and electron need to form a good-quality vertex displaced from any PV, with a flight distance greater than 15 times its uncertainty. In addition, the lifetime of the candidate is required to be greater than 0.5 ps. For the estimate of the lifetime, the Lorentz boost is calculated from the dilepton momentum, $p(e\mu)$, neglecting the contribution of the neutrino. The mass of the candidate is obtained from the dilepton system with a correction to account for not reconstructing the neutrino. The correction is inferred from the misalignment of the dilepton recon-

structed momentum and the flight direction from the PV to the decay vertex. The corrected invariant mass is computed as $m_{\rm corr} = \sqrt{m(e\mu)^2 + p(e\mu)^2 \sin^2\theta} + p(e\mu)\sin\theta$ [36], where θ is the angle formed by the dilepton momentum and the LLP flight direction. Candidates with $m_{\rm corr} < 3.3\,{\rm GeV}/c^2$ are discarded.

To suppress the heavy-flavour background the leptons are required to be isolated from other charged particles. The isolation variable is defined as $I = (\vec{p} - \vec{p}_{\rm cone})_{\rm T} \,/\, (\vec{p} + \vec{p}_{\rm cone})_{\rm T}$, where $\vec{p}$ is the momentum of the lepton candidate and $\vec{p}_{\rm cone}$ is the sum of all the momenta of charged tracks, excluding the lepton candidates, within a distance $\Delta R = \sqrt{\Delta\eta^2 + \Delta\phi^2}$ of 0.5 around the lepton, where $\Delta\eta$ and $\Delta\phi$ are the pseudorapidity and azimuthal angle differences between the lepton candidate and the charged tracks. The subscript T indicates the momentum component in the transverse plane. A value of $I = 1$ denotes a fully isolated lepton. Candidates with $I(\mu) > 0$ and $I(e) > 0.4$ are selected. Particle identification criteria are applied to the muon and the electron candidates. A tighter identification criterion on the electron is needed to reject the background due to misidentified pions or kaons. This criterion is optimised to preserve signal efficiency while maximising the rejection power over a data sample of same-sign candidates, $e^{\pm}\mu^{\pm}$, used as background proxy. The signal selection is also applied on the same-sign candidates. Figure 2 compares distributions of observables for data and simulated $b\bar{b}$ candidates, and examples of signals with different $m_{\rm LLP}$ and $\tau_{\rm LLP}$ values, which survive the selection presented above. Figure 2a, b show the candidates $m_{\rm corr}$ and flight distance distributions. These observables are used in the fit to determine the presence of signal, as explained in Sect. 5. Figure 2c, d show the transverse momentum distributions of the muon and electron, respectively. These muon and electron $p_{\rm T}$ distributions show the effect of the $p_{\rm T}$ threshold in the muon and the electron triggers. In Fig. 2e, f the distributions of the isolation variable, I, are displayed for the muon and electron, respectively. The leptons from the signal are expected to be more isolated than the ones from the $b\bar{b}$ background.

A boosted decision tree (BDT) classifier [37,38] is used to further purify the LLP $\rightarrow e^{\pm}\mu^{\mp}\nu$ candidate sample. The BDT is trained using 70k signal decays from a combination of DPP samples, and background candidates drawn from the same-sign sample. The full signal sample contains 2000 candidates for each set of ($m_{\rm LLP}$, $\tau_{\rm LLP}$) parameters. Using all simulated signal samples for the training phase allows to obtain a uniform BDT response across the ($m_{\rm LLP}$, $\tau_{\rm LLP}$) space. Furthermore, the uniformity is enforced by using a special cost function described in Ref. [39]. This cost function has the objective to provide the best classification between the signal and the background, while keeping the BDT response uniform on $m_{\rm LLP}$ and $\tau_{\rm LLP}$. The BDT input observables are: the muon $p_{\rm T}$; the maximum between the momentum of the two leptons; the two isolation variables; the angle between the muon momentum in the $e\mu$ rest frame and the $e\mu$ momentum; the ratio of the energy deposited by the muon in the calorimeters and its momentum; the ratio of the energy deposited by the electron in the HCAL and its momentum; the distance of closest approach between the two lepton tracks; the χ^2 of the LLP decay vertex; the difference between the muon and electron impact parameters divided by the LLP impact parameter; the impact parameter χ^2 of the leptons, $\chi^2_{\rm IP}(l)$, divided by $\chi^2_{\rm IP}$(LLP). For a given particle, the impact parameter χ^2 is defined as the difference between the χ^2 of the PV reconstructed with and without that particle. The BDT response, shown in Fig. 3, is uniformly distributed between 0 and 1 for the signal, while peaking at zero for the background. Candidates with a BDT value below 0.1 are rejected, leaving 61116 signal candidates. The observed BDT distribution is consistent with a $b\bar{b}$ composition of the background. Using the $b\bar{b}$ cross-section at 13 TeV measured by LHCb, $144 \pm 1 \pm 21$ μb [40], $(60 \pm 14) \times 10^3$ $b\bar{b} \rightarrow e^{\pm}\mu^{\mp}X$ candidates are predicted after selection, consistent with the observed total yield.

5 Determination of the signal yield

The signal yield is determined from a simultaneous extended maximum likelihood fit to the LLP corrected mass $m_{\rm corr}$ and flight distance distributions selected into two BDT intervals (0.1, 0.5] and (0.5, 1.0]. The study of the simulated $b\bar{b} \rightarrow e^{\pm}\mu^{\mp}X$ background indicates the presence of two components that depend on whether the two leptons belong to the same heavy-flavour jet or two different jets. The two components have different $m_{\rm corr}$ and flight distance distributions, and can be separated by the distance ΔR between the two leptons. When leptons originate from the same heavy-flavour jet, they have relatively small ΔR, selected with $\Delta R < 1$, while $\Delta R \geq 1$ selects the complementary component. The background probability density functions of the $m_{\rm corr}$ and flight distance needed in the global fit are inferred from the same-sign data. This choice has been validated by a comparison of the distributions of $m_{\rm corr}$ and the flight distance in simulated $b\bar{b} \rightarrow e^{\pm}\mu^{\mp}X$ and $b\bar{b} \rightarrow e^{\pm}\mu^{\pm}X$ candidates.

When $\Delta R < 1$, the background $m_{\rm corr}$ values are mostly found below $6\,{\rm GeV}/c^2$. This component is modelled using a sum of a Gaussian and a Crystal Ball function [41]. The fraction between the two distributions is fixed to the value obtained in the fit to the same-sign data. The parameters describing the tail are free in each BDT bin. Other parameters are free but common to all the BDT bins. For the $\Delta R \geq 1$ region $m_{\rm corr}$ is mostly above $10\,{\rm GeV}/c^2$. This region is modelled using a Johnson S_U distribution [42] with shape param-

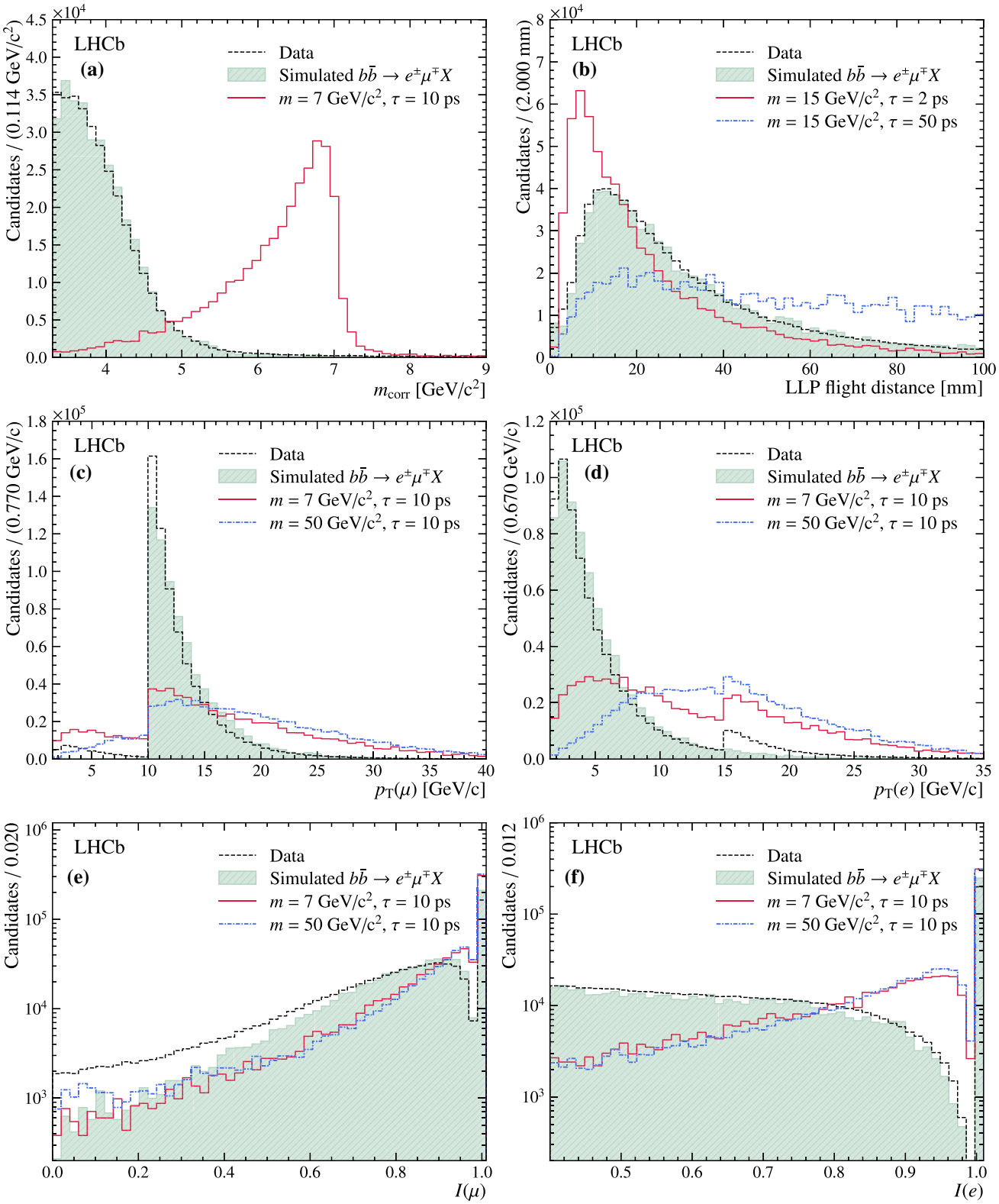

Fig. 2 Distributions in data (dashed black histogram) compared to simulated $b\bar{b} \to e^{\pm}\mu^{\mp}X$ (green filled histogram), showing, **a** $m_{\rm corr}$, **b** the LLP flight distance, **c** the transverse momentum of the muon, **d** the transverse momentum of the electron, **e** the isolation of the muon, and **f** the isolation of the electron. LLP signal distributions are also shown (coloured histograms) for different $m_{\rm LLP}$ and $\tau_{\rm LLP}$ values, where the LLP is produced through the DPP mechanism. The distributions from simulation are normalised to the number of candidates in data. There are no simulated $b\bar{b}$ candidates for $p_{\rm T}(\mu) < 10\,{\rm GeV}/c^2$ due to a $p_{\rm T}$ requirement at the generation. For the same reason there is a lack of simulated $b\bar{b}$ candidates for $p_{\rm T}(e) > 15\,{\rm GeV}/c^2$ as candidates are required to pass the muon or electron trigger

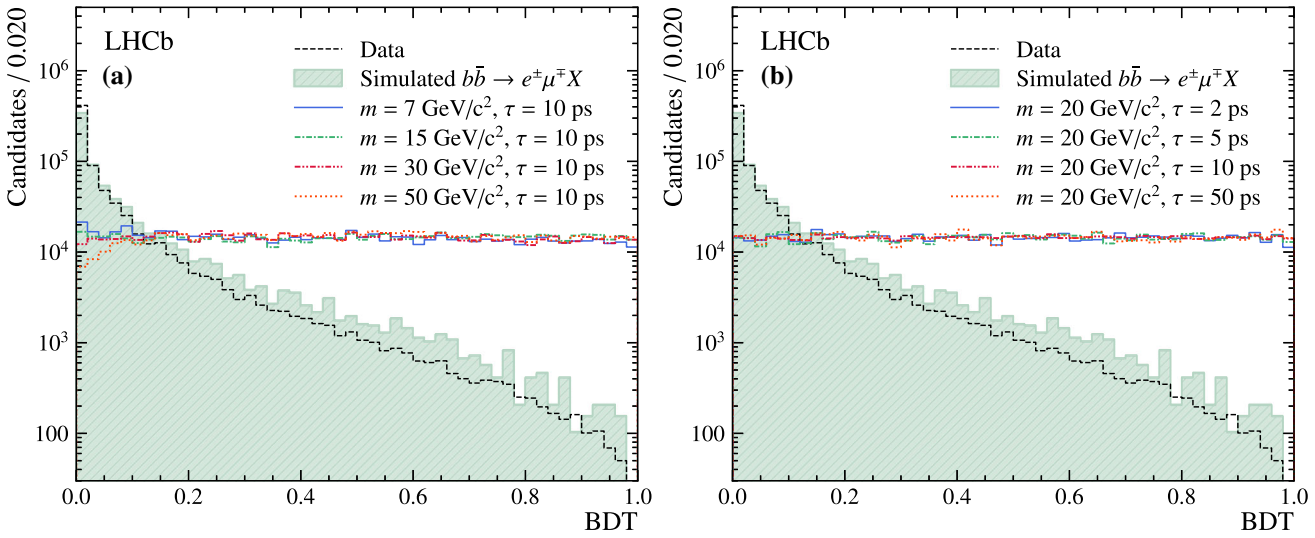

Fig. 3 Distribution of the BDT response in data (dashed black histogram) compared to simulated $b\bar{b} \to e^{\pm}\mu^{\mp}X$ (green filled histogram) and LLP signal samples (coloured histograms) for different **a** $m_{\rm LLP}$ and **b** $\tau_{\rm LLP}$ values, where the LLP is produced through the DPP mechanism. The distributions from simulation are normalised to the number of candidates in data

eters free in each BDT bin. To model the signal $m_{\rm corr}$ distribution a sum of a modified Gaussian distribution, where the left tail is exponential and the right tail a power law, and another Gaussian distribution is used. The parameters of the model are fixed to the values obtained from the fits to the simulated samples, for each ($m_{\rm LLP}$, $\tau_{\rm LLP}$) hypothesis. The same signal $m_{\rm corr}$ models are used for each BDT bin and production mechanism.

The background candidates with $\Delta R < 1$ have long flight distances, above 10 mm. The opposite is true for $\Delta R \geq 1$. The two components are modelled using a Johnson S_U distribution, with all parameters kept free. In the $\Delta R < 1$ region the parameters of the model are not shared across the BDT bins, while they are shared when $\Delta R \geq 1$. A kernel density estimation algorithm is used to estimate the probability density function of the flight distance distribution in simulated signal for each BDT bin. The same signal flight distance model for a given ($m_{\rm LLP}$, $\tau_{\rm LLP}$) hypothesis is used for each production mechanism.

In the final fit the fractions of signal yield in each BDT interval are constrained by Gaussian functions to the values and uncertainties that are estimated in the simulation. In order to explore a larger set of $m_{\rm LLP}$ values than the simulated set, signal templates for the $m_{\rm corr}$ and flight distance distributions are interpolated from the simulated distributions using a moment morphing algorithm [43]. Distributions of $m_{\rm corr}$ and the flight distance in two BDT regions are shown in Fig. 4, with an example of a fit result for a signal with $m_{\rm LLP} = 47\,{\rm GeV}/c^2$ and $\tau_{\rm LLP} = 50\,{\rm ps}$ overlaid. For each $m_{\rm LLP}$ and $\tau_{\rm LLP}$ hypothesis the fitted yields are consistent with no signal present.

6 Signal efficiencies and systematic uncertainties

The determination of the signal detection efficiency relies on simulation. Systematic effects are identified from differences between data and simulation. Regarding the electron, samples of $J/\psi \to e^+e^-$ and $Z \to e^+e^-$ decays are considered, and $J/\psi \to \mu^+\mu^-$, $\Upsilon \to \mu^+\mu^-$ and $Z \to \mu^+\mu^-$ decays are used for the muon. Samples of $b\bar{b} \to e^{\pm}\mu^{\pm}X$ candidates are used to compare distributions of the reconstructed dilepton system such as the corrected mass and the flight distance. Systematic uncertainties on the signal efficiency have been evaluated. They are summarised in Table 1 and discussed in more details below. Also reported in the table are the uncertainties on the integrated luminosity, evaluated to be 2% [44], on the signal fraction in each BDT bin, and on the signal yield associated with the fit procedure, discussed at the end of this section.

To account for the mismodelling in the simulation used to compute the signal efficiency, a bias for each variable used in the selection is determined by comparing simulated and experimental distributions of Z and $b\bar{b}$ candidates. The correlations between the selection variables are computed using the signal samples. The effect of imperfect simulation is subsequently estimated by recomputing several times the signal efficiency after changing the selection requirements on the variables by factors drawn from a multivariate normal distribution, with biases and correlations between the variables as input. The standard deviation of the distribution of efficiencies is found in the range 4.9 to 7.3%, depending on the signal mass, lifetime and production mechanism, which is taken as a contribution to the systematic uncertainty. In

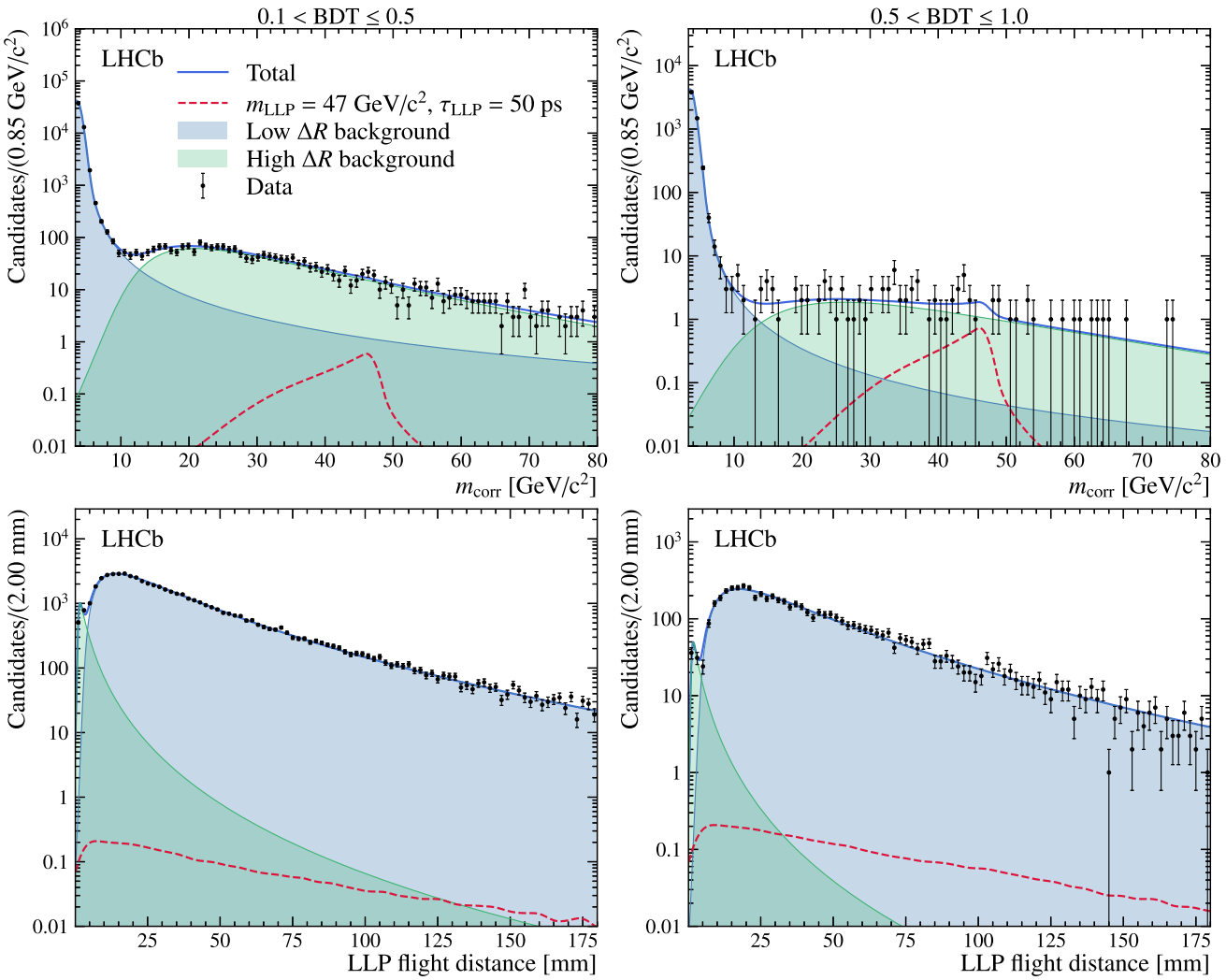

Fig. 4 Distributions of $m_{\rm corr}$ (top) and the flight distance (bottom) of two BDT intervals (left and right), where a simultaneous fit result for a LLP signal with $m_{\rm LLP} = 47\,{\rm GeV}/c^2$ and $\tau_{\rm LLP} = 50\,{\rm ps}$ is overlaid; the fitted signal yield in this example is 14 ± 14

a similar way, systematic uncertainties ranging from 0.5 to 2.4% are assigned to the identification of the two leptons.

The systematic uncertainty due to the imprecision in the simulated signal sample used to train the BDT classifier is estimated by applying the classifier on modified signal distributions: each input variable is multiplied by a scale factor drawn from a multivariate normal distribution built with the variable biases and correlations, also inferred from the control samples. The standard deviation of the efficiency distribution is used as systematic uncertainty, ranging from 0.6 to 1.0% for the BDT > 0.1 requirement, and from 3.3 to 4.0% on the signal fraction in the BDT bins.

The contribution to the systematic uncertainty from the statistical precision of the simulated signal samples is in the range 1.1–3.0%.

The theoretical uncertainties are dominated by the limited knowledge of the partonic luminosity. This contribution is estimated following the procedure explained in Ref. [45] and varies from 1.1% up to 6.1%. The minimum systematic contribution is found for the DPP and CC processes while the maximum contribution is found for the gluon-gluon fusion process HIG.

Finally, the total systematic uncertainty is obtained as the sum in quadrature of all contributions, where the different components of the detection efficiency are assumed to be fully correlated. In order to uniformly cover the full $m_{\rm LLP}$ range, a third-order polynomial is fitted to the signal detection efficiency as function of $m_{\rm LLP}$ for each simulated $\tau_{\rm LLP}$ value. A second order polynomial is also fitted to the efficiency. The difference between the two efficiencies is assigned as systematic uncertainty, a contribution that is always less than 4%. The interpolated signal efficiency for LLPs produced through the DPP mechanism is shown in Fig. 5, accounting for the geometrical acceptance. The criteria on the vertex displace-

Table 1 Contributions to the relative systematic uncertainties in %. The contributions are grouped in three categories, the integrated luminosity, the detection efficiency and the signal yield, separated by horizontal lines. The detection efficiency is affected by the parton luminosity model and depends upon the production process, with a maximum uncertainty of 6.1% for the gluon-gluon fusion process HIG

Source	Contribution (%)
Integrated luminosity	2.0
Reconstruction and selection	4.9–7.3
Particle identification	0.5–2.4
BDT	0.6–1.0
Simulation sample size	1.1–3.0
Parton luminosity	1.1–6.1
Efficiency interpolation	0.1–4.0
Signal fraction in the BDT bins	3.3–4.0
Signal model	0.7–8.1
Total	10.6–17.7

ment favour large lifetimes; however, above 10 ps the probability that the LLP decays outside the VELO increases, leading to a loss of efficiency. The selection efficiency increases with $m_{\rm LLP}$, however, this effect is counteracted by the loss of lepton candidates outside the spectrometer acceptance, which is more likely for heavier LLPs. Therefore the signal efficiencies are highest for masses between 20 and 30 GeV/c^2 and lifetimes between 5 and 10 ps. The DPP mechanism has the highest detection efficiency. On average, the detection efficiency for the HIG (CC) mechanism is 20% (60%) lower than the DPP mechanism.

The choice of templates for the corrected mass and flight distance can affect the result of the fit. The uncertainty due to the signal model accounts for imperfect simulation of the scale and resolution of the $m_{\rm corr}$ and flight distance, and that of the finite size of the simulated signal samples used to produce the probability density functions. Uncertainties of 0.2% on the $m_{\rm corr}$ scale and 1.6% on the $m_{\rm corr}$ resolution are estimated from the comparison between data and $b\bar{b}$ simulated candidates. For the flight distance a scale uncertainty of 1.2% and a resolution uncertainty of 1.1% are estimated. The propagation of uncertainties is performed using pseudo-experiments generated from the background model fitted to the same-sign data. Ten signal data points are drawn from modified signal $m_{\rm corr}$ and flight distance distributions, modified by smearing or rescaling, and added to each pseudo-experiment. The fitted signal yield is compared to the result with ten signal data points drawn from a non-modified signal. Changing the $m_{\rm corr}$ scale leads to a relative change on the signal yield from 0.1 to 1.2%, and 0.1 to 0.8% for the flight distance, depending on the signal hypothesis. A relative variation of the signal yield from 0.1 to 8.1% is observed from an additional smearing of the signal $m_{\rm corr}$ distribution, 0.1 to 0.8% for the flight distance. The effect of the limited sample size used to construct the signal model is addressed by replacing the parameter values of the signal model by values drawn from Gaussian distributions. For each parameter the mean of the Gaussian distribution is equal to its fitted value, and the standard deviation is equal to its uncertainty. A relative variation of the signal yield due to the limited sample size is found to be between 0.1 and 1.7%. A total systematic uncertainty 0.7–8.1% is accounted for the signal yield.

All the systematic uncertainties related to the integrated luminosity, the signal efficiency and the signal yield are included as nuisance parameters in the determination of the cross-section upper limits.

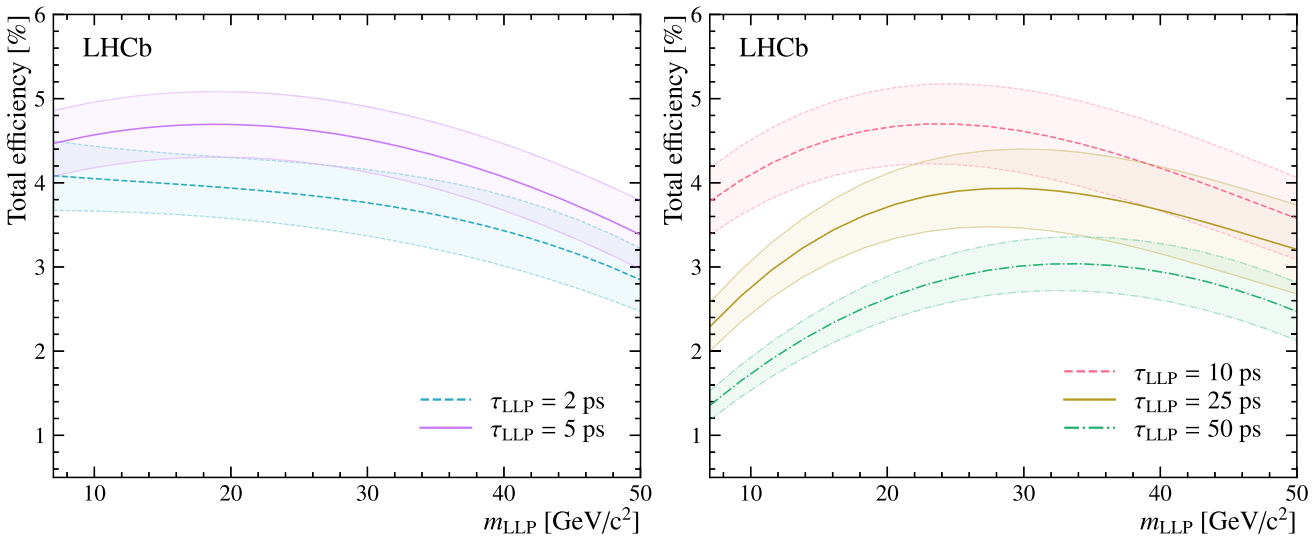

Fig. 5 Total detection efficiency for LLP produced through the DPP mechanism as a function of $m_{\rm LLP}$ (central line) and its uncertainty (coloured band), obtained for different values of $\tau_{\rm LLP}$

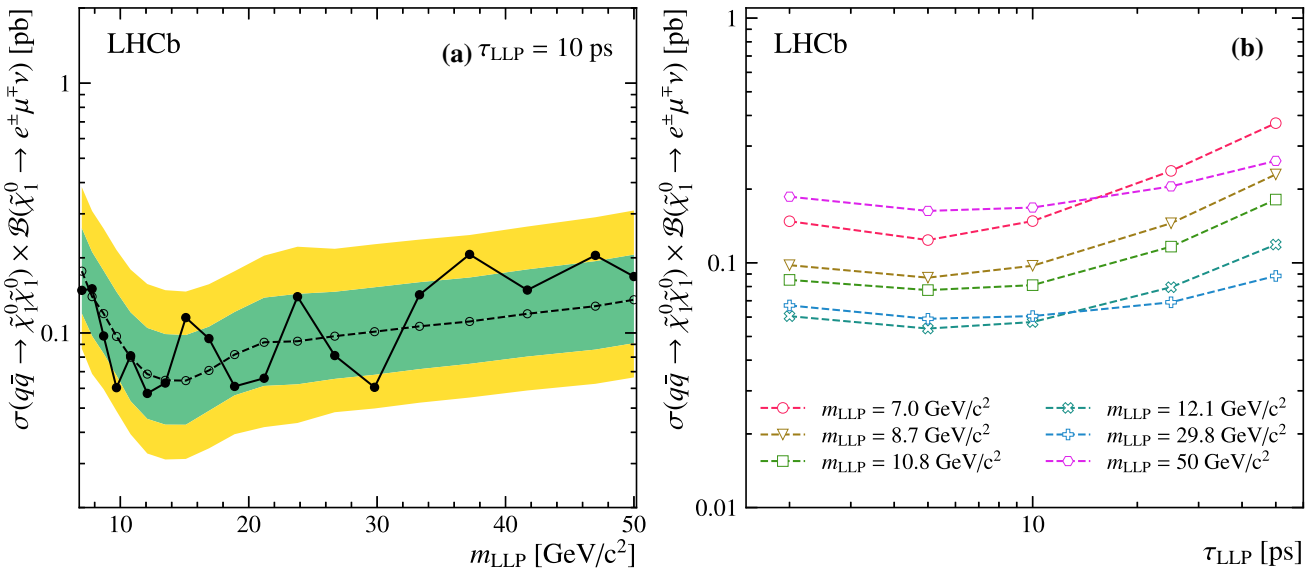

Fig. 6 **a** Expected (open circles and dotted line) and observed (filled circles and solid line) upper limits of the cross-section as a function of $m_{\rm LLP}$ for $\tau_{\rm LLP} = 10$ ps, for LLPs produced through the DPP mechanism. The green and yellow bands indicate the quantiles of the expected upper limit corresponding to $\pm 1\sigma$ and $\pm 2\sigma$ for a Gaussian distribution. **b** Observed limits on the cross-section as a function of $\tau_{\rm LLP}$ for different $m_{\rm LLP}$ values for LLPs produced through the DPP mechanism

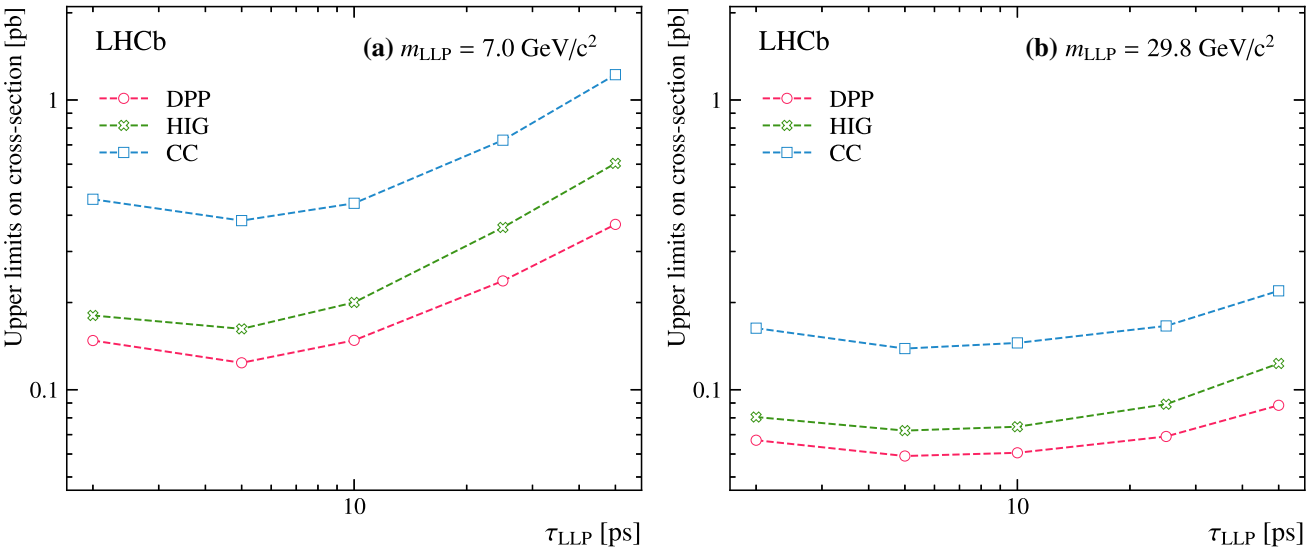

Fig. 7 Observed upper limits on the production cross-sections times branching fraction for **a** $m_{\rm LLP} = 7\,{\rm GeV}/c^2$ and **b** $m_{\rm LLP} = 29.8\,{\rm GeV}/c^2$ as function of $\tau_{\rm LLP}$ for the DPP, HIG and CC production mechanisms

7 Results

The results of the simultaneous fits to the LLP corrected mass and flight distance distributions in the two BDT intervals (0.1, 0.5] and (0.5, 1.0], are found to be compatible with the background-only hypothesis for all signal hypotheses considered. Upper limits at 95% confidence level (CL) on the production cross-sections times branching fraction are computed for each production mechanism,

$$\sigma_{\rm DPP} = \sigma(q\bar{q} \to \tilde{\chi}_1^0\tilde{\chi}_1^0) \times \mathcal{B}(\tilde{\chi}_1^0 \to e^{\pm}\mu^{\mp}\nu),$$
$$\sigma_{\rm HIG} = \sigma(gg \to h) \times \mathcal{B}(h \to \tilde{\chi}_1^0\tilde{\chi}_1^0) \times \mathcal{B}(\tilde{\chi}_1^0 \to e^{\pm}\mu^{\mp}\nu), \text{ and}$$
$$\sigma_{\rm CC} = \sigma(W \to lN) \times \mathcal{B}(N \to e^{\pm}\mu^{\mp}\nu),$$

for each pair of $m_{\rm LLP}$ and $\tau_{\rm LLP}$ values using the CLs approach [46]. Upper limits for selected $m_{\rm LLP}$ and $\tau_{\rm LLP}$ values are shown in Fig. 6, 7 and 8. Figure 6a gives examples of observed upper limits on $\sigma_{\rm DPP}$, along with the range of limits

expected for the background-only hypothesis, as a function of $m_{\rm LLP}$ for $\tau_{\rm LLP} = 10$ ps. Figure 6b shows the observed upper limits on $\sigma_{\rm DPP}$ as a function of $\tau_{\rm LLP}$, for a selection of $m_{\rm LLP}$ values that shows the range of limit values. The best observed limits on $\sigma_{\rm DPP}$ are of the order of 0.06 pb for a mass of 29.8 GeV/c^2. A comparison of observed upper limits on $\sigma_{\rm DPP}$, $\sigma_{\rm HIG}$ and $\sigma_{\rm CC}$ as a function of $\tau_{\rm LLP}$ for the lowest mass studied, $m_{\rm LLP} = 7$, and 29.8 GeV/c^2 is shown in Fig. 7. The best and worst limits are obtained for the DPP and CC mechanisms, respectively. The differences between the sensitivities for each production mechanism are principally due to detection efficiency. The limits obtained by the ATLAS experiment on the squark-antisquark production cross-section [14], where the squark has a mass of 700 or 1600 GeV/c^2 and decays to q ($\tilde{\chi}_1^0 \to ee\nu/e\mu\nu/\mu\mu\nu$), have values from 1 to 10 fb for $m(\tilde{\chi}_1^0) = 50$ GeV/c^2 in the lifetime range studied. These results are complementary to the results obtained by the ATLAS experiment, extend to lower mass and lifetime regions and explore different LLP production mechanisms.

Finally, the limits on $\sigma_{\rm HIG}$ are compared to the value of the SM Higgs boson production cross-section from gluon-gluon fusion of 48.6 ± 3.5 pb [47], which is illustrated in Fig. 8. These limits are placed on $(\sigma/\sigma^{SM}_{gg\to H}) \times \mathcal{B}(H^0 \to \tilde{\chi}_1^0\tilde{\chi}_1^0)$, assuming $\mathcal{B}(\tilde{\chi}_1^0 \to e^\pm\mu^\mp\nu) = 1$, as a function of $\tau_{\rm LLP}$ for a selection of $m_{\rm LLP}$ values. Under this assumption the limits on $\mathcal{B}(H^0 \to \tilde{\chi}_1^0\tilde{\chi}_1^0)$ have a minimum of $\sim 0.15\%$. Decays of LLP $\to \mu^+\mu^-$, produced in pairs from SM Higgs bosons, were searched by the CMS experiment [8]. Assuming $\mathcal{B}(\text{LLP} \to \mu^+\mu^-) = 1$, the limits on $\mathcal{B}(H^0 \to \text{LLP LLP})$ for $m_{\rm LLP} = 50$ GeV/c^2 are the best for lifetimes between 1 ps and 10 ns with a minimum of 0.05% [48], which is approximately 3 times lower than the minimum limits on $\mathcal{B}(H^0 \to \tilde{\chi}_1^0\tilde{\chi}_1^0)$ presented in this paper.

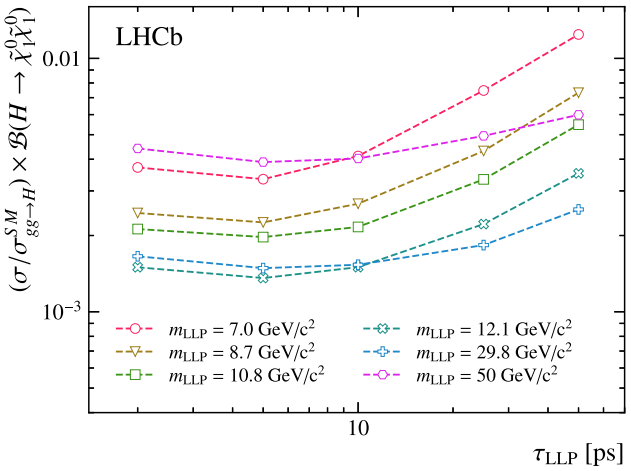

Fig. 8 Observed limits on the $(\sigma/\sigma^{SM}_{gg\to H}) \times \mathcal{B}(H^0 \to \tilde{\chi}_1^0\tilde{\chi}_1^0)$, assuming $\mathcal{B}(\tilde{\chi}_1^0 \to e^\pm\mu^\mp\nu) = 1$ as a function of $\tau_{\rm LLP}$ for different $m_{\rm LLP}$ values. The value of the gluon-gluon fusion production cross-section used is 48.6 ± 3.5 pb [47]

8 Conclusion

A search for decays of long-lived massive particles, in the $e^\pm\mu^\mp\nu$ final state, is performed using pp collisions at $\sqrt{s} =$ 13 TeV recorded with the LHCb detector, for a total integrated luminosity of 5.38 ± 0.11 fb^{-1}. The search covers LLP masses from 7 to 50 GeV/c^2, lifetimes from 2 to 50 ps and considers three production mechanisms: the direct pair production from the interaction of quarks, the pair production from the decay of a SM-like Higgs boson with a mass of 125 GeV/c^2, and the charged current production from an on-shell W boson with an additional lepton.

Fully simulated signal events are used to define the signal selection criteria and the signal detection efficiency. The background is dominated by $b\bar{b}$ candidates. A BDT, taking as input properties of the leptons and displaced vertex of the LLP, is used to purify the signal from the heavy hadron background. The signal yield is determined by a simultaneous fit of the LLP corrected mass and flight distance, using signal templates derived from simulation. All the results of the fits are compatible with the absence of signal, and upper limits on the cross-section times branching fraction for each production mechanism are computed. The best upper limits are achieved for the pair production, from interaction of quarks or the decay of a SM-like Higgs boson, for lifetimes below 10 ps and masses above 10 GeV/c^2, and are of the order of 0.1 pb.

Acknowledgements We express our gratitude to our colleagues in the CERN accelerator departments for the excellent performance of the LHC. We thank the technical and administrative staff at the LHCb institutes. We acknowledge support from CERN and from the national agencies: CAPES, CNPq, FAPERJ and FINEP (Brazil); MOST and NSFC (China); CNRS/IN2P3 (France); BMBF, DFG and MPG (Germany); INFN (Italy); NWO (Netherlands); MNiSW and NCN (Poland); MEN/IFA (Romania); MSHE (Russia); MICINN (Spain); SNSF and SER (Switzerland); NASU (Ukraine); STFC (United Kingdom); DOE NP and NSF (USA). We acknowledge the computing resources that are provided by CERN, IN2P3 (France), KIT and DESY (Germany), INFN (Italy), SURF (Netherlands), PIC (Spain), GridPP (United Kingdom), RRCKI and Yandex LLC (Russia), CSCS (Switzerland), IFIN-HH (Romania), CBPF (Brazil), PL-GRID (Poland) and OSC (USA). We are indebted to the communities behind the multiple open-source software packages on which we depend. Individual groups or members have received support from AvH Foundation (Germany); EPLANET, Marie Skłodowska-Curie Actions and ERC (European Union); A*MIDEX, ANR, Labex P2IO and OCEVU, and Région Auvergne-Rhône-Alpes (France); Key Research Program of Frontier Sciences of CAS, CAS PIFI, Thousand Talents Program, and Sci. & Tech. Program of Guangzhou (China); RFBR, RSF and Yandex LLC (Russia); GVA, XuntaGal and GENCAT (Spain); the Royal Society and the Leverhulme Trust (United Kingdom).

Data Availability Statement This manuscript has associated data in a data repository. [Authors' comment All LHCb scientific output is published in journals, with preliminary results made available in Con-

References

1. J. Alimena et al., Searching for long-lived particles beyond the Standard Model at the Large Hadron Collider. Phys. **G47**, 090501 (2020). https://doi.org/10.1088/1361-6471/ab4574J. arXiv:1903.04497
2. ATLAS collaboration, G. Aad et al., Search for pair-produced long-lived neutral particles decaying in the ATLAS hadronic calorimeter in pp collisions at $\sqrt{s} = 8$ TeV. Phys. Lett. B **743**, 15 (2015). https://doi.org/10.1016/j.physletb.2015.02.015. arXiv:1501.04020
3. ATLAS collaboration, G. Aad et al., Search for long-lived, weakly interacting particles that decay to displaced hadronic jets in proton-proton collisions at $\sqrt{s} = 8$ TeV with the ATLAS detector. Phys. Rev. D **92**, 012010 (2015). https://doi.org/10.1103/PhysRevD.92.012010. arXiv:1504.03634
4. LHCb collaboration, R. Aaij et al., Search for massive long-lived particles decaying semileptonically in the LHCb detector. Eur. Phys. J. C **77**, 224 (2017). https://doi.org/10.1140/epjc/s10052-017-4744-6. arXiv:1612.00945
5. LHCb collaboration, R. Aaij et al., Updated search for long-lived particles decaying to jet pairs. Eur. Phys. J. C **77**, 812 (2017). https://doi.org/10.1140/epjc/s10052-017-5178-x. arXiv:1705.07332
6. LHCb collaboration, R. Aaij et al., Search for Higgs-like boson decaying into pair of long-lived particles. Eur. Phys. J. C **76**, 664 (2016). https://doi.org/10.1140/epjc/s10052-016-4489-7. arXiv:1609.03124
7. ATLAS collaboration, M. Aaboud et al., Search for the Higgs boson produced in association with a vector boson and decaying into two spin-zero particles in the $H \to aa \to 4b$ channel in pp collisions at $\sqrt{s} = 13$ TeV with the ATLAS detector. **10**, 031 (2018). https://doi.org/10.1007/JHEP10(2018)031JHEP. arXiv:1806.07355
8. CMS collaboration, V. Khachatryan et al., Search for long-lived particles that decay into final states containing two electrons or two muons in proton-proton collisions at $\sqrt{s} = 8$ TeV. Phys. Rev. D **91**, 052012 (2015). https://doi.org/10.1103/PhysRevD.91.052012. arXiv:1411.6977
9. ATLAS collaboration, M. Aaboud et al., Search for long-lived particles in final states with displaced dimuon vertices in pp collisions at $\sqrt{s} = 13$ TeV with the ATLAS detector. Phys. Rev. D **99**, 012001 (2019). https://doi.org/10.1103/PhysRevD.99.012001. arXiv:1808.03057
10. S.P. Martin, A supersymmetry primer. Adv. Ser. Direct. High Energy Phys. **21**, 1 (2010). https://doi.org/10.1142/9789812839657_0001. arXiv:hep-ph/9709356
11. R.N. Mohapatra, G. Senjanović, Neutrino mass and spontaneous parity nonconservation. Phys. Rev. Lett. **44**, 912 (1980). https://doi.org/10.1103/PhysRevLett.44.912
12. T. Yanagida, Horizontal symmetry and masses of neutrinos. Prog. Theor. Phys. **64**, 1103 (1980). https://doi.org/10.1143/PTP.64.1103
13. M. Gell-Mann, P. Ramond, R. Slansky, Complex spinors and unified theories. Conf. Proc. C **790927**, 315 (1979). arXiv:1306.4669
14. ATLAS collaboration, G. Aad et al., Search for displaced vertices of oppositely charged leptons from decays of long-lived particles in pp collisions at $\sqrt{s} = 13$ TeV with the ATLAS detector, Phys. Lett. B **801**, 135114 (2020). https://doi.org/10.1016/j.physletb.2019.135114. arXiv:1907.10037
15. ATLAS collaboration, G. Aad et al., Search for heavy neutral leptons in decays of W bosons produced in 13 TeV pp collisions using prompt and displaced signatures with the ATLAS detector. JHEP **10**, 265 (2019). https://doi.org/10.1007/JHEP10(2019)265. arXiv:1905.09787
16. LHCb collaboration, R. Aaij et al., Search for $A' \to \mu^+\mu^-$ decays. Phys. Rev. Lett. **124**, 041801 (2020). https://doi.org/10.1103/PhysRevLett.124.041801. arXiv:1910.06926
17. LHCb collaboration, R. Aaij et al., Search for Majorana neutrinos in $B^- \to \pi^+\mu^-\mu^-$ decays, Phys. Rev. Lett. **112**, 131802 (2014). https://doi.org/10.1103/PhysRevLett.112.131802. arXiv:1401.5361
18. LHCb collaboration, R. Aaij et al., Search for hidden-sector bosons in $B^0 \to K^{*0}\mu^+\mu^-$ decays. Phys. Rev. Lett. **115**, 161802 (2015). https://doi.org/10.1103/PhysRevLett.115.161802. arXiv:1508.04094
19. LHCb collaboration, A.A. Alves Jr. et al., The LHCb detector at the LHC. JINST **3**, S08005 (2008). https://doi.org/10.1088/1748-0221/3/08/S08005
20. LHCb collaboration, R. Aaij et al., LHCb detector performance. Int. J. Mod. Phys. A **30**, 1530022 (2015). https://doi.org/10.1142/S0217751X15300227. arXiv:1412.6352
21. G. Dujany, B. Storaci, Real-time alignment and calibration of the LHCb Detector in Run II. J. Phys. Conf. Ser. **664**, 082010 (2015). https://doi.org/10.1088/1742-6596/664/8/082010
22. J. Alwall et al., The automated computation of tree-level and next-to-leading order differential cross sections, and their matching to parton shower simulations. JHEP **07**, 079 (2014). https://doi.org/10.1007/JHEP07(2014)079. arXiv:1405.0301
23. C. Degrande et al., UFO—the universal FeynRules output. Comput. Phys. Commun. **183**, 1201 (2012). https://doi.org/10.1016/j.cpc.2012.01.022. arXiv:1108.2040
24. J.C. Pati, A. Salam, Lepton number as the fourth "color". Phys. Rev. D **10**, 275 (1974). https://doi.org/10.1103/PhysRevD.10.275
25. R.N. Mohapatra, J.C. Pati, "Natural" left-right symmetry. Phys. Rev. D **11**, 2558 (1975). https://doi.org/10.1103/PhysRevD.11.2558 **(cited By 1155)**
26. G. Senjanovic, R.N. Mohapatra, Exact left-right symmetry and spontaneous violation of parity. Phys. Rev. D **12**, 1502 (1975). https://doi.org/10.1103/PhysRevD.12.1502 **(cited By 1583)**
27. P. Artoisenet, R. Frederix, O. Mattelaer, R. Rietkerk, Automatic spin-entangled decays of heavy resonances in Monte Carlo simulations. JHEP **03**, 015 (2013). https://doi.org/10.1007/JHEP03(2013)015. arXiv:1212.3460
28. T. Sjöstrand, S. Mrenna, P. Skands, PYTHIA 6.4 physics and manual. JHEP **05**, 026 (2006). https://doi.org/10.1088/1126-6708/2006/05/026. arXiv:hep-ph/0603175
29. T. Sjöstrand, S. Mrenna, P. Skands, A brief introduction to PYTHIA 8.1. Comput. Phys. Commun **178**, 852 (2008). https://doi.org/10.1016/j.cpc.2008.01.036. arXiv:0710.3820

32. Geant4 collaboration, J. Allison et al., Geant4 developments and applications. IEEE Trans. Nucl. Sci. **53**, 270 (2006). https://doi.org/10.1109/TNS.2006.869826
33. Geant4 collaboration, S. Agostinelli et al., Geant4: a simulation toolkit. Nucl. Instrum. Methods A **506**, 250 (2003). https://doi.org/10.1016/S0168-9002(03)01368-8
34. M. Clemencic et al., The LHCb simulation application, Gauss: design, evolution and experience. J. Phys. Conf. Ser. **331**, 032023 (2011). https://doi.org/10.1088/1742-6596/331/3/032023
35. LHCb collaboration, R. Aaij et al., Measurement of the $B^0 \to K^{*0} e^+ e^-$ branching fraction at low dilepton mass. JHEP **05**, 159 (2013). https://doi.org/10.1007/JHEP05(2013)159. arXiv:1304.3035
36. SLD collaboration, K. Abe et al., A measurement of R(b) using a vertex mass tag. Phys. Rev. Lett. **80**, 660 (1998). https://doi.org/10.1103/PhysRevLett.80.660. arXiv:hep-ex/9708015
37. L. Breiman, J.H. Friedman, R.A. Olshen, C.J. Stone, *Classification and Regression Trees* (Wadsworth international group, Belmont, 1984)
38. Y. Freund, R.E. Schapire, A decision-theoretic generalization of on-line learning and an application to boosting. J. Comput. Syst. Sci. **55**, 119 (1997). https://doi.org/10.1006/jcss.1997.1504
39. A. Rogozhnikov, Reweighting with boosted decision trees. J. Phys. Conf. Ser. **762**, 012036 (2016). https://doi.org/10.1088/1742-6596/762/1/012036. arXiv:1608.05806. https://github.com/arogozhnikov/hep_ml
40. LHCb collaboration, R. Aaij et al., Measurement of the b-quark-quark production cross-section in 7 and 13TeV collisions. Phys. Rev. Lett. **118**, 052002 (2017). https://doi.org/10.1103/PhysRevLett.118.052002. arXiv:1612.05140. Erratum ibid. **119**, 169901 (2017). https://doi.org/10.1103/PhysRevLett.119.169901
41. T. Skwarnicki, A study of the radiative cascade transitions between the Upsilon-prime and Upsilon resonances. PhD thesis, Institute of Nuclear Physics, Krakow (1986). http://inspirehep.net/record/230779/DESY-F31-86-02
42. N.L. Johnson, Systems of frequency curves generated by methods of translation. Biometrika **36**, 149 (1949)
43. M. Baak, S. Gadatsch, R. Harrington, W. Verkerke, Interpolation between multi-dimensional histograms using a new non-linear moment morphing method. Nucl. Instrum. Methods A **771**, 39 (2014). https://doi.org/10.1016/j.nima.2014.10.033
44. LHCb collaboration, R. Aaij et al., Precision luminosity measurements at LHCb. JINST **9**, P12005 (2014). https://doi.org/10.1088/1748-0221/9/12/P12005. arXiv:1410.0149
45. J. Butterworth et al., PDF4LHC recommendations for LHC Run II. J. Phys. G **43**, 023001 (2016). https://doi.org/10.1088/0954-3899/43/2/023001. arXiv:1510.03865
46. A.L. Read, Presentation of search results: the CL_s technique. J. Phys. G **28**, 2693 (2002). https://doi.org/10.1088/0954-3899/28/10/313
47. M. Cepeda et al., Report from Working Group 2: Higgs physics at the HL-LHC and HE-LHC. CERN Yellow Rep. Monogr. **7**, 221 (2019). https://doi.org/10.23731/CYRM-2019-007.221. arXiv:1902.00134
48. L. Lee, C. Ohm, A. Soffer, T.-T. Yu, Collider searches for long-lived particles beyond the Standard Model. Prog. Part. Nucl. Phys. **106**, 210 (2019). https://doi.org/10.1016/j.ppnp.2019.02.006. arXiv:1810.12602

LHCb Collaboration

R. Aaij[31], C. Abellán Beteta[49], T. Ackernley[59], B. Adeva[45], M. Adinolfi[53], H. Afsharnia[9], C. A. Aidala[84], S. Aiola[25], Z. Ajaltouni[9], S. Akar[64], J. Albrecht[14], F. Alessio[47], M. Alexander[58], A. Alfonso Albero[44], Z. Aliouche[61], G. Alkhazov[37], P. Alvarez Cartelle[47], S. Amato[2], Y. Amhis[11], L. An[21], L. Anderlini[21], A. Andreianov[37], M. Andreotti[20], F. Archilli[16], A. Artamonov[43], M. Artuso[67], K. Arzymatov[41], E. Aslanides[10], M. Atzeni[49], B. Audurier[11], S. Bachmann[16], M. Bachmayer[48], J. J. Back[55], S. Baker[60], P. Baladron Rodriguez[45], V. Balagura[11], W. Baldini[20], J. Baptista Leite[1], R. J. Barlow[61], S. Barsuk[11], W. Barter[60], M. Bartolini[23,i], F. Baryshnikov[80], J. M. Basels[13], G. Bassi[28], B. Batsukh[67], A. Battig[14], A. Bay[48], M. Becker[14], F. Bedeschi[28], I. Bediaga[1], A. Beiter[67], V. Belavin[41], S. Belin[26], V. Bellee[48], K. Belous[43], I. Belov[39], I. Belyaev[38], G. Bencivenni[22], E. Ben-Haim[12], A. Berezhnoy[39], R. Bernet[49], D. Berninghoff[16], H. C. Bernstein[67], C. Bertella[47], E. Bertholet[12], A. Bertolin[27], C. Betancourt[49], F. Betti[19,e], M. O. Bettler[54], Ia. Bezshyiko[49], S. Bhasin[53], J. Bhom[33], L. Bian[72], M. S. Bieker[14], S. Bifani[52], P. Billoir[12], M. Birch[60], F. C. R. Bishop[54], A. Bizzeti[21,s], M. Bjørn[62], M. P. Blago[47], T. Blake[55], F. Blanc[48], S. Blusk[67], D. Bobulska[58], J. A. Boelhauve[14], O. Boente Garcia[45], T. Boettcher[63], A. Boldyrev[81], A. Bondar[42,v], N. Bondar[37], S. Borghi[61], M. Borisyak[41], M. Borsato[16], J. T. Borsuk[33], S. A. Bouchiba[48], T. J. V. Bowcock[59], A. Boyer[47], C. Bozzi[20], M. J. Bradley[60], S. Braun[65], A. Brea Rodriguez[45], M. Brodski[47], J. Brodzicka[33], A. Brossa Gonzalo[55], D. Brundu[26], A. Buonaura[49], C. Burr[47], A. Bursche[26], A. Butkevich[40], J. S. Butter[31], J. Buytaert[47], W. Byczynski[47], S. Cadeddu[26], H. Cai[72], R. Calabrese[20,g], L. Calefice[14], L. Calero Diaz[22], S. Cali[22], R. Calladine[52], M. Calvi[24,j], M. Calvo Gomez[83], P. Camargo Magalhaes[53], A. Camboni[44], P. Campana[22], D. H. Campora Perez[47], A. F. Campoverde Quezada[5], S. Capelli[24,j], L. Capriotti[19,e], A. Carbone[19,e], G. Carboni[29], R. Cardinale[23,i], A. Cardini[26], I. Carli[6], P. Carniti[24,j], L. Carus[13], K. Carvalho Akiba[31], A. Casais Vidal[45], G. Casse[59], M. Cattaneo[47], G. Cavallero[47], S. Celani[48], J. Cerasoli[10], A. J. Chadwick[59], M. G. Chapman[53], M. Charles[12], Ph. Charpentier[47], G. Chatzikonstantinidis[52], C. A. Chavez Barajas[59], M. Chefdeville[8], C. Chen[3], S. Chen[26], A. Chernov[33], S.-G. Chitic[47], V. Chobanova[45], S. Cholak[48], M. Chrzaszcz[33], A. Chubykin[37], V. Chulikov[37], P. Ciambrone[22], M. F. Cicala[55], X. Cid Vidal[45], G. Ciezarek[47], P. E. L. Clarke[57], M. Clemencic[47], H. V. Cliff[54], J. Closier[47], J. L. Cobbledick[61], V. Coco[47], J. A. B. Coelho[11], J. Cogan[10], E. Cogneras[9], L. Cojocariu[36], P. Collins[47], T. Colombo[47], L. Congedo[18], A. Contu[26], N. Cooke[52], G. Coombs[58], G. Corti[47], C. M. Costa Sobral[55], B. Couturier[47], D. C. Craik[63], J. Crkovská[66], M. Cruz Torres[1], R. Currie[57], C. L. Da Silva[66], E. Dall'Occo[14], J. Dalseno[45], C. D'Ambrosio[47],

A. Danilina[38], P. d'Argent[47], A. Davis[61], O. De Aguiar Francisco[61], K. De Bruyn[77], S. De Capua[61], M. De Cian[48], J. M. De Miranda[1], L. De Paula[2], M. De Serio[18,d], D. De Simone[49], P. De Simone[22], J. A. de Vries[78], C. T. Dean[66], W. Dean[84], D. Decamp[8], L. Del Buono[12], B. Delaney[54], H.-P. Dembinski[14], A. Dendek[34], V. Denysenko[49], D. Derkach[81], O. Deschamps[9], F. Desse[11], F. Dettori[26,f], B. Dey[72], P. Di Nezza[22], S. Didenko[80], L. Dieste Maronas[45], H. Dijkstra[47], V. Dobishuk[51], A. M. Donohoe[17], F. Dordei[26], A. C. dos Reis[1], L. Douglas[58], A. Dovbnya[50], A. G. Downes[8], K. Dreimanis[59], M. W. Dudek[33], L. Dufour[47], V. Duk[76], P. Durante[47], J. M. Durham[66], D. Dutta[61], M. Dziewiecki[16], A. Dziurda[33], A. Dzyuba[37], S. Easo[56], U. Egede[68], V. Egorychev[38], S. Eidelman[42,v], S. Eisenhardt[57], S. Ek-In[48], L. Eklund[58], S. Ely[67], A. Ene[36], E. Epple[66], S. Escher[13], J. Eschle[49], S. Esen[31], T. Evans[47], A. Falabella[19], J. Fan[3], Y. Fan[5], B. Fang[72], N. Farley[52], S. Farry[59], D. Fazzini[24,j], P. Fedin[38], M. Féo[47], P. Fernandez Declara[47], A. Fernandez Prieto[45], J. M. Fernandez-tenllado Arribas[44], F. Ferrari[19,e], L. Ferreira Lopes[48], F. Ferreira Rodrigues[2], S. Ferreres Sole[31], M. Ferrillo[49], M. Ferro-Luzzi[47], S. Filippov[40], R. A. Fini[18], M. Fiorini[20,g], M. Firlej[34], K. M. Fischer[62], C. Fitzpatrick[61], T. Fiutowski[34], F. Fleuret[11,b], M. Fontana[47], F. Fontanelli[23,i], R. Forty[47], V. Franco Lima[59], M. Franco Sevilla[65], M. Frank[47], E. Franzoso[20], G. Frau[16], C. Frei[47], D. A. Friday[58], J. Fu[25], Q. Fuehring[14], W. Funk[47], E. Gabriel[31], T. Gaintseva[41], A. Gallas Torreira[45], D. Galli[19,e], S. Gambetta[57], Y. Gan[3], M. Gandelman[2], P. Gandini[25], Y. Gao[4], M. Garau[26], L. M. Garcia Martin[55], P. Garcia Moreno[44], J. García Pardiñas[49], B. Garcia Plana[45], F. A. Garcia Rosales[11], L. Garrido[44], D. Gascon[44], C. Gaspar[47], R. E. Geertsema[31], D. Gerick[16], L. L. Gerken[14], E. Gersabeck[61], M. Gersabeck[61], T. Gershon[55], D. Gerstel[10], Ph. Ghez[8], V. Gibson[54], M. Giovannetti[22,k], A. Gioventù[45], P. Gironella Gironell[44], L. Giubega[36], C. Giugliano[20,g], K. Gizdov[57], E. L. Gkougkousis[47], V. V. Gligorov[12], C. Göbel[69], E. Golobardes[83], D. Golubkov[38], A. Golutvin[60,80], A. Gomes[1,a], S. Gomez Fernandez[44], F. Goncalves Abrantes[69], M. Goncerz[33], G. Gong[3], P. Gorbounov[38], I. V. Gorelov[39], C. Gotti[24,j], E. Govorkova[31], J. P. Grabowski[16], R. Graciani Diaz[44], T. Grammatico[12], L. A. Granado Cardoso[47], E. Graugés[44], E. Graverini[48], G. Graziani[21], A. Grecu[36], L. M. Greeven[31], P. Griffith[20], L. Grillo[61], S. Gromov[80], L. Gruber[47], B. R. Gruberg Cazon[62], C. Gu[3], M. Guarise[20], P. A. Günther[16], E. Gushchin[40], A. Guth[13], Y. Guz[43,47], T. Gys[47], T. Hadavizadeh[68], G. Haefeli[48], C. Haen[47], J. Haimberger[47], S. C. Haines[54], T. Halewood-leagas[59], P. M. Hamilton[65], Q. Han[7], X. Han[16], T. H. Hancock[62], S. Hansmann-Menzemer[16], N. Harnew[62], T. Harrison[59], C. Hasse[47], M. Hatch[47], J. He[5], M. Hecker[60], K. Heijhoff[31], K. Heinicke[14], A. M. Hennequin[47], K. Hennessy[59], L. Henry[25,46], J. Heuel[13], A. Hicheur[2], D. Hill[62], M. Hilton[61], S. E. Hollitt[14], P. H. Hopchev[48], J. Hu[16], J. Hu[71], W. Hu[7], W. Huang[5], X. Huang[72], W. Hulsbergen[31], R. J. Hunter[55], M. Hushchyn[81], D. Hutchcroft[59], D. Hynds[31], P. Ibis[14], M. Idzik[34], D. Ilin[37], P. Ilten[64], A. Inglessi[37], A. Ishteev[80], K. Ivshin[37], R. Jacobsson[47], S. Jakobsen[47], E. Jans[31], B. K. Jashal[46], A. Jawahery[65], V. Jevtic[14], M. Jezabek[33], F. Jiang[3], M. John[62], D. Johnson[47], C. R. Jones[54], T. P. Jones[55], B. Jost[47], N. Jurik[47], S. Kandybei[50], Y. Kang[3], M. Karacson[47], M. Karpov[81], N. Kazeev[81], F. Keizer[47,54], M. Kenzie[55], T. Ketel[32], B. Khanji[47], A. Kharisova[82], S. Kholodenko[43], K. E. Kim[67], T. Kirn[13], V. S. Kirsebom[48], O. Kitouni[63], S. Klaver[31], K. Klimaszewski[35], S. Koliiev[51], A. Kondybayeva[80], A. Konoplyannikov[38], P. Kopciewicz[34], R. Kopecna[16], P. Koppenburg[31], M. Korolev[39], I. Kostiuk[31,51], O. Kot[51], S. Kotriakhova[30,37], P. Kravchenko[37], L. Kravchuk[40], R. D. Krawczyk[47], M. Kreps[55], F. Kress[60], S. Kretzschmar[13], P. Krokovny[42,v], W. Krupa[34], W. Krzemien[35], W. Kucewicz[1,33], M. Kucharczyk[33], V. Kudryavtsev[42,v], H. S. Kuindersma[31], G. J. Kunde[66], T. Kvaratskheliya[38], D. Lacarrere[47], G. Lafferty[61], A. Lai[26], A. Lampis[26], D. Lancierini[49], J. J. Lane[61], R. Lane[53], G. Lanfranchi[22], C. Langenbruch[13], J. Langer[14], O. Lantwin[49,80], T. Latham[55], F. Lazzari[28,t], R. Le Gac[10], S. H. Lee[84], R. Lefèvre[9], A. Leflat[39], S. Legotin[80], O. Leroy[10], T. Lesiak[33], B. Leverington[16], H. Li[71], L. Li[62], P. Li[16], X. Li[66], Y. Li[6], Y. Li[6], Z. Li[67], X. Liang[67], T. Lin[60], R. Lindner[47], V. Lisovskyi[14], R. Litvinov[26], G. Liu[71], H. Liu[5], S. Liu[6], X. Liu[3], A. Loi[26], J. Lomba Castro[45], I. Longstaff[58], J. H. Lopes[2], G. Loustau[49], G. H. Lovell[54], Y. Lu[6], D. Lucchesi[27,m], S. Luchuk[40], M. Lucio Martinez[31], V. Lukashenko[31], Y. Luo[3], A. Lupato[61], E. Luppi[20,g], O. Lupton[55], A. Lusiani[28,r], X. Lyu[5], L. Ma[6], S. Maccolini[19,e], F. Machefert[11], F. Maciuc[36], V. Macko[48], P. Mackowiak[14], S. Maddrell-Mander[53], O. Madejczyk[34], L. R. Madhan Mohan[53], O. Maev[37], A. Maevskiy[81], D. Maisuzenko[37], M. W. Majewski[34], J. J. Malczewski[33], S. Malde[62], B. Malecki[47], A. Malinin[79], T. Maltsev[42,v], H. Malygina[16], G. Manca[26,f], G. Mancinelli[10], R. Manera Escalero[44], D. Manuzzi[19,e], D. Marangotto[25,o], J. Maratas[9,u], J. F. Marchand[8], U. Marconi[19], S. Mariani[21,47,h], C. Marin Benito[11], M. Marinangeli[48,*], P. Marino[48], J. Marks[16], P. J. Marshall[59], G. Martellotti[30], L. Martinazzoli[47,j], M. Martinelli[24,j], D. Martinez Santos[45], F. Martinez Vidal[46], A. Massafferri[1], M. Materok[13], R. Matev[47], A. Mathad[49], Z. Mathe[47], V. Matiunin[38], C. Matteuzzi[24], K. R. Mattioli[84], A. Mauri[31], E. Maurice[11,b], J. Mauricio[44], M. Mazurek[35], M. McCann[60], L. Mcconnell[17], T. H. Mcgrath[61], A. McNab[61], R. McNulty[17], J. V. Mead[59], B. Meadows[64], C. Meaux[10], G. Meier[14], N. Meinert[75], D. Melnychuk[35], S. Meloni[24,j], M. Merk[31,78], A. Merli[25], L. Meyer Garcia[2], M. Mikhasenko[47], D. A. Milanes[73], E. Millard[55], M. Milovanovic[47], M.-N. Minard[8], L. Minzoni[20,g], S. E. Mitchell[57], B. Mitreska[61], D. S. Mitzel[47], A. Mödden[14], R. A. Mohammed[62], R. D. Moise[60], T. Mombächer[14], I. A. Monroy[73], S. Monteil[9], M. Morandin[27], G. Morello[22], M. J. Morello[28,r], J. Moron[34], A. B. Morris[74], A. G. Morris[55], R. Mountain[67], H. Mu[3],

F. Muheim[57], M. Mukherjee[7], M. Mulder[47], D. Müller[47], K. Müller[49], C. H. Murphy[62], D. Murray[61], P. Muzzetto[26], P. Naik[53], T. Nakada[48], R. Nandakumar[56], T. Nanut[48], I. Nasteva[2], M. Needham[57], I. Neri[20,g], N. Neri[25,o], S. Neubert[74], N. Neufeld[47], R. Newcombe[60], T. D. Nguyen[48], C. Nguyen-Mau[48], E. M. Niel[11], S. Nieswand[13], N. Nikitin[39], N. S. Nolte[47], C. Nunez[84], A. Oblakowska-Mucha[34], V. Obraztsov[43], D. P. O'Hanlon[53], R. Oldeman[26,f], M. E. Olivares[67], C. J. G. Onderwater[77], A. Ossowska[33], J. M. Otalora Goicochea[2], T. Ovsiannikova[38], P. Owen[49], A. Oyanguren[46,47], B. Pagare[55], P. R. Pais[47], T. Pajero[28,47,r], A. Palano[18], M. Palutan[22], Y. Pan[61], G. Panshin[82], A. Papanestis[56], M. Pappagallo[18,d], L. L. Pappalardo[20,g], C. Pappenheimer[64], W. Parker[65], C. Parkes[61], C. J. Parkinson[45], B. Passalacqua[20], G. Passaleva[21], A. Pastore[18], M. Patel[60], C. Patrignani[19,e], C. J. Pawley[78], A. Pearce[47], A. Pellegrino[31], M. Pepe Altarelli[47], S. Perazzini[19], D. Pereima[38], P. Perret[9], K. Petridis[53], A. Petrolini[23,i], A. Petrov[79], S. Petrucci[57], M. Petruzzo[25], T. T. H. Pham[67], A. Philippov[41], L. Pica[28], M. Piccini[76], B. Pietrzyk[8], G. Pietrzyk[48], M. Pili[62], D. Pinci[30], J. Pinzino[47], F. Pisani[47], A. Piucci[16], Resmi P.K[10], V. Placinta[36], S. Playfer[57], J. Plews[52], M. Plo Casasus[45], F. Polci[12], M. Poli Lener[22], M. Poliakova[67], A. Poluektov[10], N. Polukhina[80,c], I. Polyakov[67], E. Polycarpo[2], G. J. Pomery[53], S. Ponce[47], A. Popov[43], D. Popov[5,47], S. Popov[41], S. Poslavskii[43], K. Prasanth[33], L. Promberger[47], C. Prouve[45], V. Pugatch[51], A. Puig Navarro[49], H. Pullen[62], G. Punzi[28,n], W. Qian[5], J. Qin[5], R. Quagliani[12], B. Quintana[8], N. V. Raab[17], R. I. Rabadan Trejo[10], B. Rachwal[34], J. H. Rademacker[53], M. Rama[28], M. Ramos Pernas[55], M. S. Rangel[2], F. Ratnikov[41,81], G. Raven[32], M. Reboud[8], F. Redi[48], F. Reiss[12], C. Remon Alepuz[46], Z. Ren[3], V. Renaudin[62], R. Ribatti[28], S. Ricciardi[56], K. Rinnert[59], P. Robbe[11], A. Robert[12], G. Robertson[57], A. B. Rodrigues[48], E. Rodrigues[59], J. A. Rodriguez Lopez[73], A. Rollings[62], P. Roloff[47], V. Romanovskiy[43], M. Romero Lamas[45], A. Romero Vidal[45], J. D. Roth[84], M. Rotondo[22], M. S. Rudolph[67], T. Ruf[47], J. Ruiz Vidal[46], A. Ryzhikov[81], J. Ryzka[34], J. J. Saborido Silva[45], N. Sagidova[37], N. Sahoo[55], B. Saitta[26,f], D. Sanchez Gonzalo[44], C. Sanchez Gras[31], R. Santacesaria[30], C. Santamarina Rios[45], M. Santimaria[22], E. Santovetti[29,k], D. Saranin[80], G. Sarpis[61], M. Sarpis[74], A. Sarti[30], C. Satriano[30,q], A. Satta[29], M. Saur[5], D. Savrina[38,39], H. Sazak[9], L. G. Scantlebury Smead[62], S. Schael[13], M. Schellenberg[14], M. Schiller[58], H. Schindler[47], M. Schmelling[15], T. Schmelzer[14], B. Schmidt[47], O. Schneider[48], A. Schopper[47], M. Schubiger[31], S. Schulte[48], M. H. Schune[11], R. Schwemmer[47], B. Sciascia[22], A. Sciubba[30], S. Sellam[45], A. Semennikov[38], M. Senghi Soares[32], A. Sergi[47,52], N. Serra[49], J. Serrano[10], L. Sestini[27], A. Seuthe[14], P. Seyfert[47], D. M. Shangase[84], M. Shapkin[43], I. Shchemerov[80], L. Shchutska[48], T. Shears[59], L. Shekhtman[42,v], Z. Shen[4], V. Shevchenko[79], E. B. Shields[24,j], E. Shmanin[80], J. D. Shupperd[67], B. G. Siddi[20], R. Silva Coutinho[49], G. Simi[27], S. Simone[18,d], I. Skiba[20,g], N. Skidmore[74], T. Skwarnicki[67], M. W. Slater[52], J. C. Smallwood[62], J. G. Smeaton[54], A. Smetkina[38], E. Smith[13], M. Smith[60], A. Snoch[31], M. Soares[19], L. Soares Lavra[9], M. D. Sokoloff[64], F. J. P. Soler[58], A. Solovev[37], I. Solovyev[37], F. L. Souza De Almeida[2], B. Souza De Paula[2], B. Spaan[14], E. Spadaro Norella[25,o], P. Spradlin[58], F. Stagni[47], M. Stahl[64], S. Stahl[47], P. Stefko[48], O. Steinkamp[49,80], S. Stemmle[16], O. Stenyakin[43], H. Stevens[14], S. Stone[67], M. E. Stramaglia[48], M. Straticiuc[36], D. Strekalina[80], S. Strokov[82], F. Suljik[62], J. Sun[26], L. Sun[72], Y. Sun[65], P. Svihra[61], P. N. Swallow[52], K. Swientek[34], A. Szabelski[35], T. Szumlak[34], M. Szymanski[47], S. Taneja[61], Z. Tang[3], T. Tekampe[14], F. Teubert[47], E. Thomas[47], K. A. Thomson[59], M. J. Tilley[60], V. Tisserand[9], S. T'Jampens[8], M. Tobin[6], S. Tolk[47], L. Tomassetti[20,g], D. Torres Machado[1], D. Y. Tou[12], M. Traill[58], M. T. Tran[48], E. Trifonova[80], C. Trippl[48], A. Tsaregorodtsev[10], G. Tuci[28,n], A. Tully[48], N. Tuning[31], A. Ukleja[35], D. J. Unverzagt[16], E. Ursov[80], A. Usachov[31], A. Ustyuzhanin[41,81], U. Uwer[16], A. Vagner[82], V. Vagnoni[19], A. Valassi[47], G. Valenti[19], N. Valls Canudas[44], M. van Beuzekom[31], M. Van Dijk[48], H. Van Hecke[66], E. van Herwijnen[80], C. B. Van Hulse[17], M. van Veghel[77], R. Vazquez Gomez[45], P. Vazquez Regueiro[45], C. Vázquez Sierra[31], S. Vecchi[20], J. J. Velthuis[53], M. Veltri[21,p], A. Venkateswaran[67], M. Veronesi[31], M. Vesterinen[55], D. Vieira[64], M. Vieites Diaz[48], H. Viemann[75], X. Vilasis-Cardona[83], E. Vilella Figueras[59], P. Vincent[12], G. Vitali[28], A. Vollhardt[49], D. Vom Bruch[12], A. Vorobyev[37], V. Vorobyev[42,v], N. Voropaev[37], R. Waldi[75], J. Walsh[28], C. Wang[16], J. Wang[3], J. Wang[72], J. Wang[4], J. Wang[6], M. Wang[3], R. Wang[53], Y. Wang[7], Z. Wang[49], H. M. Wark[59], N. K. Watson[52], S. G. Weber[12], D. Websdale[60], C. Weisser[63], B. D. C. Westhenry[53], D. J. White[61], M. Whitehead[53], D. Wiedner[14], G. Wilkinson[62], M. Wilkinson[67], I. Williams[54], M. Williams[63,68], M. R. J. Williams[57], F. F. Wilson[56], W. Wislicki[35], M. Witek[33], L. Witola[16], G. Wormser[11], S. A. Wotton[54], H. Wu[67], K. Wyllie[47], Z. Xiang[5], D. Xiao[7], Y. Xie[7], H. Xing[71], A. Xu[4], J. Xu[5], L. Xu[3], M. Xu[7], Q. Xu[5], Z. Xu[5], Z. Xu[4], D. Yang[3], Y. Yang[5], Z. Yang[3], Z. Yang[65], Y. Yao[67], L. E. Yeomans[59], H. Yin[7], J. Yu[70], X. Yuan[67], O. Yushchenko[43], E. Zaffaroni[48], K. A. Zarebski[52], M. Zavertyaev[15,c], M. Zdybal[33], O. Zenaiev[47], M. Zeng[3], D. Zhang[7], L. Zhang[3], S. Zhang[4], Y. Zhang[47], Y. Zhang[62], A. Zhelezov[16], Y. Zheng[5], X. Zhou[5], Y. Zhou[5], X. Zhu[3], V. Zhukov[13,39], J. B. Zonneveld[57], S. Zucchelli[19,e], D. Zuliani[27], G. Zunica[61]

[1] Centro Brasileiro de Pesquisas Físicas (CBPF), Rio de Janeiro, Brazil
[2] Universidade Federal do Rio de Janeiro (UFRJ), Rio de Janeiro, Brazil
[3] Center for High Energy Physics, Tsinghua University, Beijing, China

[4] School of Physics State Key Laboratory of Nuclear Physics and Technology, Peking University, Beijing, China
[5] University of Chinese Academy of Sciences, Beijing, China
[6] Institute Of High Energy Physics (IHEP), Beijing, China
[7] Institute of Particle Physics, Central China Normal University, Wuhan, Hubei, China
[8] Univ. Grenoble Alpes, Univ. Savoie Mont Blanc, CNRS, IN2P3-LAPP, Annecy, France
[9] Université Clermont Auvergne, CNRS/IN2P3, LPC, Clermont-Ferrand, France
[10] Aix Marseille Univ, CNRS/IN2P3, CPPM, Marseille, France
[11] Université Paris-Saclay, CNRS/IN2P3, IJCLab, Orsay, France
[12] LPNHE, Sorbonne Université, Paris Diderot Sorbonne Paris Cité, CNRS/IN2P3, Paris, France
[13] I. Physikalisches Institut, RWTH Aachen University, Aachen, Germany
[14] Fakultät Physik, Technische Universität Dortmund, Dortmund, Germany
[15] Max-Planck-Institut für Kernphysik (MPIK), Heidelberg, Germany
[16] Physikalisches Institut, Ruprecht-Karls-Universität Heidelberg, Heidelberg, Germany
[17] School of Physics, University College Dublin, Dublin, Ireland
[18] INFN Sezione di Bari, Bari, Italy
[19] INFN Sezione di Bologna, Bologna, Italy
[20] INFN Sezione di Ferrara, Ferrara, Italy
[21] INFN Sezione di Firenze, Florence, Italy
[22] INFN Laboratori Nazionali di Frascati, Frascati, Italy
[23] INFN Sezione di Genova, Genoa, Italy
[24] INFN Sezione di Milano-Bicocca, Milan, Italy
[25] INFN Sezione di Milano, Milan, Italy
[26] INFN Sezione di Cagliari, Monserrato, Italy
[27] Universita degli Studi di Padova, Universita e INFN, Padova, Padua, Italy
[28] INFN Sezione di Pisa, Pisa, Italy
[29] INFN Sezione di Roma Tor Vergata, Rome, Italy
[30] INFN Sezione di Roma La Sapienza, Rome, Italy
[31] Nikhef National Institute for Subatomic Physics, Amsterdam, The Netherlands
[32] Nikhef National Institute for Subatomic Physics, VU University Amsterdam, Amsterdam, The Netherlands
[33] Henryk Niewodniczanski Institute of Nuclear Physics Polish Academy of Sciences, Kraków, Poland
[34] Faculty of Physics and Applied Computer Science, AGH-University of Science and Technology, Kraków, Poland
[35] National Center for Nuclear Research (NCBJ), Warsaw, Poland
[36] Horia Hulubei National Institute of Physics and Nuclear Engineering, Bucharest-Magurele, Romania
[37] Petersburg Nuclear Physics Institute NRC Kurchatov Institute (PNPI NRC KI), Gatchina, Russia
[38] Institute of Theoretical and Experimental Physics NRC Kurchatov Institute (ITEP NRC KI), Moscow, Russia
[39] Institute of Nuclear Physics, Moscow State University (SINP MSU), Moscow, Russia
[40] Institute for Nuclear Research of the Russian Academy of Sciences (INR RAS), Moscow, Russia
[41] Yandex School of Data Analysis, Moscow, Russia
[42] Budker Institute of Nuclear Physics (SB RAS), Novosibirsk, Russia
[43] Institute for High Energy Physics NRC Kurchatov Institute (IHEP NRC KI), Protvino, Russia, Protvino, Russia
[44] ICCUB, Universitat de Barcelona, Barcelona, Spain
[45] Instituto Galego de Física de Altas Enerxías (IGFAE), Universidade de Santiago de Compostela, Santiago de Compostela, Spain
[46] Instituto de Fisica Corpuscular, Centro Mixto Universidad de Valencia-CSIC, Valencia, Spain
[47] European Organization for Nuclear Research (CERN), Geneva, Switzerland
[48] Institute of Physics, Ecole Polytechnique Fédérale de Lausanne (EPFL), Lausanne, Switzerland
[49] Physik-Institut, Universität Zürich, Zurich, Switzerland
[50] NSC Kharkiv Institute of Physics and Technology (NSC KIPT), Kharkiv, Ukraine
[51] Institute for Nuclear Research of the National Academy of Sciences (KINR), Kyiv, Ukraine
[52] University of Birmingham, Birmingham, UK
[53] H.H. Wills Physics Laboratory, University of Bristol, Bristol, UK
[54] Cavendish Laboratory, University of Cambridge, Cambridge, UK
[55] Department of Physics, University of Warwick, Coventry, UK

[56] STFC Rutherford Appleton Laboratory, Didcot, UK
[57] School of Physics and Astronomy, University of Edinburgh, Edinburgh, UK
[58] School of Physics and Astronomy, University of Glasgow, Glasgow, UK
[59] Oliver Lodge Laboratory, University of Liverpool, Liverpool, UK
[60] Imperial College London, London, UK
[61] Department of Physics and Astronomy, University of Manchester, Manchester, UK
[62] Department of Physics, University of Oxford, Oxford, UK
[63] Massachusetts Institute of Technology, Cambridge, MA, USA
[64] University of Cincinnati, Cincinnati, OH, USA
[65] University of Maryland, College Park, MD, USA
[66] Los Alamos National Laboratory (LANL), Los Alamos, USA
[67] Syracuse University, Syracuse, NY, USA
[68] School of Physics and Astronomy, Monash University, Melbourne, Australia
[69] Pontifícia Universidade Católica do Rio de Janeiro (PUC-Rio), Rio de Janeiro, Brazil
[70] Physics and Micro Electronic College, Hunan University, Changsha City, China
[71] Guangdong Provencial Key Laboratory of Nuclear Science, Institute of Quantum Matter, South China Normal University, Guangzhou, China
[72] School of Physics and Technology, Wuhan University, Wuhan, China
[73] Departamento de Fisica , Universidad Nacional de Colombia, Bogotá, Colombia
[74] Helmholtz-Institut für Strahlen und Kernphysik, Universität Bonn, Bonn, Germany
[75] Institut für Physik, Universität Rostock, Rostock, Germany
[76] INFN Sezione di Perugia, Perugia, Italy
[77] Van Swinderen Institute, University of Groningen, Groningen, The Netherlands
[78] Universiteit Maastricht, Maastricht, The Netherlands
[79] National Research Centre Kurchatov Institute, Moscow, Russia
[80] National University of Science and Technology "MISIS", Moscow, Russia
[81] National Research University Higher School of Economics, Moscow, Russia
[82] National Research Tomsk Polytechnic University, Tomsk, Russia
[83] DS4DS, La Salle, Universitat Ramon Llull, Barcelona, Spain
[84] University of Michigan, Ann Arbor, USA

[a] Universidade Federal do Triângulo Mineiro (UFTM), Uberaba-MG, Brazil
[b] Laboratoire Leprince-Ringuet, Palaiseau, France
[c] P.N. Lebedev Physical Institute, Russian Academy of Science (LPI RAS), Moscow, Russia
[d] Università di Bari, Bari, Italy
[e] Università di Bologna, Bologna, Italy
[f] Università di Cagliari, Cagliari, Italy
[g] Università di Ferrara, Ferrara, Italy
[h] Università di Firenze, Florence, Italy
[i] Università di Genova, Genoa, Italy
[j] Università di Milano Bicocca, Milan, Italy
[k] Università di Roma Tor Vergata, Rome, Italy
[l] AGH - University of Science and Technology, Faculty of Computer Science, Electronics and Telecommunications, Kraków, Poland
[m] Università di Padova, Padua, Italy
[n] Università di Pisa, Pisa, Italy
[o] Università degli Studi di Milano, Milan, Italy
[p] Università di Urbino, Urbino, Italy
[q] Università della Basilicata, Potenza, Italy
[r] Scuola Normale Superiore, Pisa, Italy
[s] Università di Modena e Reggio Emilia, Modena, Italy

[t] Università di Siena, Siena, Italy
[u] MSU - Iligan Institute of Technology (MSU-IIT), Iligan, Philippines
[v] Novosibirsk State University, Novosibirsk, Russia